# First-principles and classical molecular dynamics simulation of shocked polymers

Thomas R. Mattsson,[1] J. Matthew D. Lane,[1] Kyle R. Cochrane,[2] Michael P. Desjarlais,[1] Aidan P. Thompson,[1] Flint Pierce,[1,3] and Gary S. Grest[1]

[1]*Sandia National Laboratories, Albuquerque, New Mexico 87185, USA*

[2]*Ktech Corporation, Albuquerque, New Mexico 87123, USA*

[3]*Department of Chemistry, Clemson University, Clemson, South Carolina 29634, USA*

(Received 22 December 2009; published 3 February 2010)

Density functional theory (DFT) molecular dynamics (MD) and classical MD simulations of the principal shock Hugoniot are presented for two hydrocarbon polymers, polyethylene (PE) and poly(4-methyl-1-pentene) (PMP). DFT results are in excellent agreement with experimental data, which is currently available up to 80 GPa. Further, we predict the PE and PMP Hugoniots up to 350 and 200 GPa, respectively. For comparison, we studied two reactive and two nonreactive interaction potentials. For the latter, the exp-6 interaction of Borodin *et al.* showed much better agreement with experiment than OPLS. For the reactive force fields, ReaxFF displayed decidedly better agreement than AIREBO. For shocks above 50 GPa, only the DFT results are of high fidelity, establishing DFT as a reliable method for shocked macromolecular systems.

DOI: 10.1103/PhysRevB.81.054103 PACS number(s): 82.35.Lr, 31.15.E−, 62.50.Ef, 71.15.Pd

## I. INTRODUCTION

Over the last few years, first-principles simulations in combination with increasingly accurate shock experiments at multi-Mbar pressure have yielded important insights into how matter behaves under extreme conditions. While comprehensive advances have been made for many light elements, for example deuterium[1,2] and carbon,[3] progress has been slower for equally important, albeit more challenging, materials such as molecular crystals and polymers.[4]

Modeling a macromolecular material requires trade offs in system size and fidelity of the atomic interaction. It is not clear *a priori* how to best strike the balance between the competing requirements, since the critical variable determining system response may in some cases be the size-specific structure/geometry, or in other cases the bond reactivity and interaction fidelity. In order to resolve this important question, we have simulated shock compression of two different polymers using first-principles density functional theory[5] (DFT) and classical molecular dynamics (MD) simulations using four different interaction potentials, ReaxFF,[6] AIREBO,[7] OPLS,[8] and Borodin *et al.*'s exp-6 potentials.[9]

For generality, we chose to study two polymers, polyethylene (PE) and poly(4-methyl-1-pentene) (PMP or TPX). PE is an extensively used general-purpose plastic with the simplest possible linear alkane structure. Atactic PMP is commonly used in shock studies as a low-density polymer foam and has specialized applications in target materials for inertially confined fusion (ICF) studies. PMP is a branched alkane with a bulky side chain. The two polymers were selected to be representative of two different classes of polymers, as PMP is amorphous at room temperature, while PE is semicrystalline. We believe the results are likely to be widely applicable to other macromolecular materials. Several experimental studies of shocked PE have been reported[10–13] in addition to the quantitative data for both PE and PMP from the LASL shock handbook.[14]

This paper is organized into five sections. Section II extensively describes our modeling techniques for polymer interactions, describing the DFT calculations, the reactive and nonreactive MD interaction potentials, and the construction of the simulation material. Section III describes the methods used to arrive at Hugoniot shock states. Section IV details the results of both quantum and classical calculations for PE and PMP; comparison with previous experimental results is provided for pressure, while, temperature results as a function of shock strength are compared for the different simulation potentials; and finally a discussion of chemical structure and shock-induced dissociation is presented. Section V summarizes the work and concludes.

## II. MODELING POLYMER INTERACTIONS

While DFT is a computationally costly method in which it is necessary to reduce the number of simulation atoms to several hundred at most, it allows for a high-fidelity description of chemical bonds and interatomic repulsion. Reactive force fields such as ReaxFF[6] and AIREBO,[7] which have been applied to study shocks in hydrocarbons,[15–17] cannot accurately capture the range of responses compared to DFT, however they allow for chemical reactions and significantly larger system sizes. Nonreactive force fields, such the OPLS potential of Jorgensen *et al.*[8] and the exp-6 potential of Borodin *et al.*,[9] are computationally much more efficient and allow for even larger system sizes, but do not allow covalent bonds to break or form, which can become important for strong shocks. The relative speed of the different methods is naturally of interest: OPLS and exp-6 are the fastest potentials, AIREBO is approximately twice as slow while ReaxFF is 30 times slower than OPLS and exp-6. All classical MD simulations were run in LAMMPS[18,19] while the DFT-MD simulations were performed with VASP 5.1.40.[20,21]

### A. Density functional theory with AM05

DFT is a formally exact representation of the Schrödinger equation. However, in practice, the choice of exchange-correlation functional determines the accuracy. We employed

 

the recently developed multipurpose Armiento-Mattsson (AM05) functional;[22] it is a functional with no empirically determined parameters. It improves upon the local density approximation (LDA) by reproducing two model systems with known solutions: the uniform electron gas and the surface jellium.[22,23] AM05 has demonstrated high fidelity for many solids;[23,24] in Ref. 23 the performance of seven functionals was compared for twenty representative semiconductors, simple metals, transition metals, alkali-halides, and oxides. For AM05, the prediction bias (mean average error) in lattice constant is small while LDA and PBE both exhibit significant bias. On average, AM05 is better than choosing between LDA and PBE for each solid separately (Table I of Ref. 23) and does as well as the decidedly more computationally demanding hybrid functionals studied in Refs. 25 and 26. Furthermore, AM05 also works well for hydrogen bonding in the water dimer[27] and for chemical reaction energies for a large number of molecular reactions.[28]

Both polyethylene and poly(4-methyl-1-pentene) are materials where van der Waals forces are important. Although previous work using DFT by Byrd and Rice demonstrated a difficulty in modeling energetic molecular solids at low pressure, they found an increasing accuracy as the external pressure increases,[29] and the behavior under strong shocks is dominated by the high pressure response. Furthermore, the lack of van der Waals attraction in AM05[24] makes it decidedly different from most other exchange-correlation functionals. Since the functional displays a monotonic behavior upon expansion and compression,[24] it is arguably suitable for studying compression in van der Waals systems. The applicability of AM05 to shocked energetic materials will be the subject of future work.[30]

Finally, AM05 was recently the best suited functional to model quartz[31] up to 1 TPa in the development of a high-pressure shock impedance standard. Taken together, there are ample reasons not only to employ AM05, but to expect high-fidelity results for shock compression.

The DFT-MD simulations were performed with VASP 5.1.40[20,21] using stringent convergence settings.[2,32,33] The plane wave cutoff was above 800 eV in order to converge the stress-tensor.[2,34] Pulay errors are minimal due to the high cutoff and the appreciable changes in volume for the different calculations along the Hugoniot.[35] The ionic timestep is between 0.1 and 0.5 fs depending on temperature. Steady-state simulations in the NVT ensemble used a Nosé-Hoover thermostat with a time constant of 80 timesteps. Velocities were scaled to control temperature in the ramped-temperature simulations. Partition of kinetic energy between hydrogen and carbon was verified by monitoring the temperature for each element separately.[36] Complex $k$-point sampling with mean-value point $(\frac{1}{4},\frac{1}{4},\frac{1}{4})$ was used due to its high accuracy for disordered structures at high temperature. Electronic states were occupied according to Mermin's finite-temperature formulation of DFT,[37] a factor that is particularly important in the warm-dense matter regime where thermal effects are significant.

### B. Reactive interaction potentials

ReaxFF and AIREBO are reactive potentials which allow the possibility of dynamic bond formation and breaking. ReaxFF uses bond order and charge equilibration to model local chemical changes. It has been used to simulate a wide variety of materials and processes, including molecular solids under shock and detonation.[17,38,39] AIREBO is based on Brenner's REBO potential augmented with explicit 6–12 dispersion terms and has previously been used to model shock propagation in short chain hydrocarbons.[15,16]

Both the AIREBO and ReaxFF calculations were performed using the standard LAMMPS parallel implementations,[19] which have been validated against the original serial codes. For AIREBO, a 10.2 Å cutoff was used. For ReaxFF, a 10 Å cutoff was used and the charge equilibration convergence tolerance was set to $10^{-6}$. The specific form of the ReaxFF potential in LAMMPS is described in Chenoweth *et al.*[6] The ReaxFF parameter values are those proveded with the LAMMPS code package[19] and for hydrocarbons they give similar results as the parameters used by Strachan *et al.*[38]

### C. Nonreactive interaction potentials

The OPLS and exp-6 potentials have preassigned nonbreakable bonds. In these potentials, interactions within and between molecules are described by a set of atomic potentials which include van der Waals, electrostatic, molecular bond, angle, and torsion interaction terms. The total energy $U_{tot}$ is given by

$$U_{tot} = U_{\text{nonbond}} + U_{\text{bond}} + U_{\text{ang}} + U_{\text{tor}}, \tag{1}$$

where $U_{\text{nonbond}}$ is the sum of the van der Waals and Coulomb potentials. The bond potential and angle potential are harmonic. The dihedral potentials for the OPLS and exp-6 force fields differ only slightly in form.

An important difference between these potentials is in the form of the nonbonded interactions. The OPLS nonbonded potential is composed of standard 12–6 Lennard-Jones (LJ) and Coulomb potentials,[8,40] while the exp-6 force field of Borodin *et al.*[9] utilizes a Buckingham exponential-6 form for the nonbonded pair potential. Nonbonded interactions are calculated between all atom pairs within different molecules and between distant atoms within the same molecule. The respective functional forms are

$$U_{\text{nonbond}}^{\text{OPLS}} = 4\epsilon_{ij}\left[\left(\frac{\sigma_{ij}}{r_{ij}}\right)^{12} - \left(\frac{\sigma_{ij}}{r_{ij}}\right)^{6}\right] + k_{\text{coul}}\frac{q_i q_j}{r_{ij}}, \tag{2}$$

and

$$U_{\text{nonbond}}^{\text{exp-6}} = A_{ij}\exp(-B_{ij}r_{ij}) - \frac{C_{ij}}{r_{ij}^6}, \tag{3}$$

where $\epsilon_{ij}$ sets the energy scale, $\sigma_{ij}$ sets the separation scale for the $ij$ pair, $q$ is partial charge. $A_{ij}$ is the strength of the potential's repulsive component, $B_{ij}^{-1}$ is the characteristic decay length, and $C_{ij}$ indicates the strength and range of the attractive component. The atoms in the exp-6 potential are uncharged. Both potentials were cut off at 12 Å for the large simulation cells. An 8 Å cutoff was used to equilibrate the smallest PMP system before running in DFT. The different behavior under compression is shown in Fig. 1 and is a most

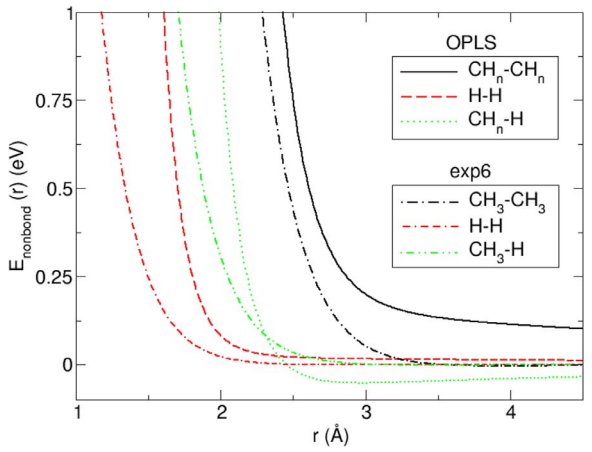


FIG. 1. (Color online) Nonbonded contributions to the OPLS and exp-6 potential for C-C, C-H, and H-H. For C-H and H-H pairs, the OPLS repulsive component is significantly larger than for exp-6 potential, with the largest difference being in H-H.

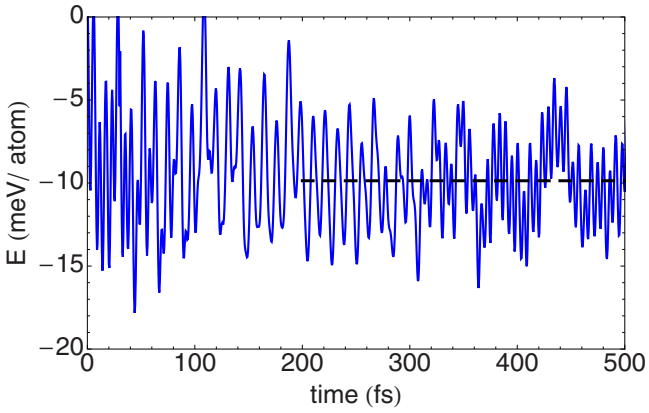


FIG. 2. (Color online) Electronic energy in meV per atom as a function of timestep in a DFT-AM05 simulation when starting from a PMP configuration taken from a classical MD run with the exp-6 potential (blue full line). Velocities were reinitialized randomly at 300 K. The black dashed line is the average energy over the entire 4000 step simulation. The adjustment in energy when going from the exp-6 potential to DFT-AM05 is less than 10 meV/atom.

likely reason for the stark differences in shock pressure between the two.

Long-range Coulomb corrections were included using the particle-particle-particle-mesh (PPPM) method.[41] A complete set of OPLS and exp-6 force-field parameters used in this study can be found in Ref. 42.

### D. Construction of the simulation cells

#### 1. Polyethylene

Two periodic crystalline PE samples of different sizes were constructed. The larger sample was built using Accelrys Materials Studio[43] with the polymer builder module and converted to a LAMMPS data structure. It consisted of 168 chains of $C_{44}H_{88}$ in a triangular lattice. This larger system, with 22 176 atoms, was used for all four classical potentials. For each potential, the sample was re-equilibrated at 300 K and constant pressure to produce an initial state for the shock runs. The initial densities for the shock-ready PE samples were $\rho_{0,\mathrm{OPLS}}=0.986$ g/cm$^3$, $\rho_{0,\text{exp-6}}=0.962$ g/cm$^3$, $\rho_{0,\mathrm{ReaxFF}}=0.930$ g/cm$^3$, and $\rho_{0,\mathrm{AIREBO}}=0.915$ g/cm$^3$.

The smaller crystalline PE sample used in the DFT simulations was built entirely within VASP. It consisted of 4 chains of hexadecane, $C_{16}H_{34}$ with 200 total atoms in a tetragonal unit cell. To produce the reference state the unit cell lattice *c*/*a* ratio was adjusted in steps until the stress was minimized while maintaining volume at a density of $\rho_{0,\mathrm{DFT}}=0.955$ g/cm$^3$. Reference energy and pressure were obtained by equilibration for 11 ps.

#### 2. Poly(4-methyl-1-pentene)

Two periodic amorphous PMP samples of different sizes were constructed. Both samples were built using Accelrys Materials Studio with the polymer and amorphous cell builder modules and converted either to a LAMMPS or VASP data structure. The larger sample consisted of 50 atactic chains of 50 repeat units for a total of 45 100 atoms. Equilibrated samples at pressure of 1 bar and $T=300$ K were produced for each classical potential. The OPLS sample was obtained by equilibrating at 600 K for 5 ns and cooling to 300 K over 15 ns at a constant pressure of 1 bar. The exp-6 shock-ready state was re-equilibrated for 3 ns from the OPLS state. Similarly, the AIREBO and ReaxFF systems were obtained from the equilibrated exp-6 system. The initial densities for the shock-ready PMP samples were $\rho_{0,\mathrm{OPLS}}=0.822$ g/cm$^3$, $\rho_{0,\text{exp-6}}=0.829$ g/cm$^3$, $\rho_{0,\mathrm{ReaxFF}}=0.801$ g/cm$^3$, and $\rho_{0,\mathrm{AIREBO}}=0.756$ g/cm$^3$. This underestimation of $\rho_{0,\mathrm{AIREBO}}$ for AIREBO is consistent with previous results that found that this potential overestimated the pressure at ambient density for a number of short linear and branched alkanes.[7,44] A generalization[44] of AIREBO, which allows the LJ $\sigma$ and $\epsilon$ parameters to each depend on local hybridization has been shown to predict more accurately the pressure at ambient density. However since it still employs the LJ 12–6 form for the interaction, it is not likely to do significantly better at high density than the original version.

The smaller sample consisted of 440 atoms in 4 atactic chains of 6 repeat units in a cubic cell. This sample was equilibrated at 600 K, then cooled to 300 K over 1–2 ns with the exp-6 potential. Two geometries each served as input to the DFT simulations. One was rethermalized in VASP at 500 K then cooled to 300 K, the second was continued directly. The energy shift from this initial exp-6 equilibrated state to the DFT equilibrated state was less than 10 meV/atom (from −5.6799 to −5.6808 eV/atom). Thus, near ambient conditions ($\rho_{0,\mathrm{DFT}}=0.83$ g/cm$^3$), the DFT methods and nonreactive classical potentials produce nearly identical reference configurations. Figure 2 shows a DFT-AM05 simulation continuing a pre-equilibrated simulation using the exp-6 potential. The energy shift is less than 10 meV/atom, demonstrating that it is possible to switch between the two descriptions in the normal state ($\rho=0.83$ g cm$^{-3}$) with negligible change in energy. Since the exp-6 potential reproduces thermodynamic properties for hydrocarbon polymers very well, the agreement supports the use of AM05 for this class of systems. The reference energy and pressure was obtained over a

4 ps equilibrated simulation after rethermalization within DFT at 500 K followed by annealing to 300 K.

## III. MODELING SHOCK RESPONSE

A shock changes the thermodynamic state of a material; the density $\rho$, pressure $P$, internal energy $U$, and temperature $T$ all jump to new values behind the shock front. Although the detailed time-resolved behavior of a shock wave is complex, the Hugoniot state itself is a state in thermodynamic equilibrium with well-defined thermodynamic properties. We have used two methods to determine the shocked state.

### A. Principal Hugoniot—thermodynamic equilibrium

In all DFT simulations, the principal Hugoniot curve is mapped by applying the hydrostatic Rankine-Hugoniot equation,

$$(U - U_0) = \frac{1}{2}(P + P_0)(V_0 - V), \tag{4}$$

which is valid for a solid when the applied stress greatly exceeds the yield stress.[45] It relates the final thermodynamic state variables far behind a planar shock wave for a given set of initial thermodynamic state variables. These thermodynamic variables are the initial and final internal energies $U_0$ and $U$, respectively; the pressures $P_0$ and $P$; and, the volumes $V_0$ and $V$.

The DFT Hugoniot points were found using an iterative compression procedure beginning from an equilibrated initial reference state. To determine each Hugoniot state point, the system was instantaneously compressed isotropically and allowed to equilibrate. The ionic and electronic temperatures are then ramped at a rate of between 0.3–1.0 K/fs, depending on the temperature range, until the *sampled* thermodynamic variables satisfied Eq. (4). To verify these ramped-temperature Hugoniot points, several densities were simulated for long times (tens of ps) in the *NVT* ensemble, at temperatures just above and below the Hugoniot temperature allowing the Hugoniot pressure to be interpolated.

### B. Principal Hugoniot—using dynamic control

Classical MD Hugoniot points were produced using a modification of the constant stress uniaxial Hugoniostat ($NP_{zz}Hug$) method of Ravelo *et al.*,[46] replacing their integral feedback (Nose-Hoover dynamics) with linear feedback (Berendsen dynamics), in order to avoid oscillatory transients. The relaxation time constants were set to 200 ps for the nonreactive potentials and 20 ps for the reactive potentials. Simulation durations varied depending on the potentials (ranging from 200 ps to 2 ns), and were selected to guarantee that steady final strains and internal energies had reached the values predicted by Eq. (4).

Since the modeling methods required slightly different procedures for MD versus DFT calculations, we verified that the results were not overly sensitive to these differences. For example, for the exp-6 potential at target pressures of 40 GPa for PMP, we found that using the DFT procedure (i.e., a single compression stage followed by a temperature ramp) applied to the MD system gave Hugoniot pressures within 1.5% of the result of the Hugoniostat procedure.

## IV. RESULTS

In traditional flyer plate impact experiments, the pressure and density can be straightforwardly deduced from measurements of shock transit times and/or direct shock speeds in combination with shock impedance matching using a known standard.[31] Measuring the temperature, on the other hand, remains a sizeable experimental challenge. In simulations, thermodynamic variables such as temperature, internal energy, pressure, and specific heat are readily accessible. While the calculated pressure/density relationship of the principal Hugoniot can be directly compared to experiments, the resulting calculated shock temperatures are used to better understand the final state as well as develop equation of state models. The chemical composition of the material is also accessible from simulations, providing additional information about phase transitions and chemical changes taking place under shock conditions.

### A. Shock pressure

The main focus of this work is a detailed comparison of calculated shock pressure with existing experimental data and predictions for multi-Mbar shocks. As stated in the introduction, DFT has demonstrated high fidelity for shock compression of many elements and compounds, for example deuterium,[2] carbon,[3] quartz,[31] water,[47] and liquid xenon.[48] However, it was not clear, *a priori* whether one could expect similar agreement between simulation and experiment for polymer systems. Complications might have arisen from long relaxation times, or from polymers systems' significant van der Waals force contributions, which often dominate over covalent bond forces.

#### *1. Polyethylene*

The experimental data presented for shocked PE in Fig. 3 is taken from the LASL shock handbook.[14] The data is for samples with an initial average density of 0.916 $g/cm^3$. The later high-pressure experiments[10] were performed on samples with a higher initial average density (0.952 $g/cm^3$). Although a small difference, we adjusted for it in Fig. 3 by scaling the shock handbook data to the nominal density of semicrystalline PE (0.955 $g/cm^3$) as follows: $\rho' = \rho_0 u_s/(u_s - u_p)$ and $P = \rho_0 u_s u_p$, where $\rho_0$ is the new reference density and $u_s$ (shock velocity) and $u_p$(particle velocity) are the experimental data in Ref. 14. Likewise, the theoretical results of Ref. 4 are scaled to the nominal density of semicrystalline PE.

Our PE Hugoniot results, (see Fig. 3) demonstrate that for shocks above 50 GPa, which leads to a final state density of $\sim$1.9 $g/cm^3$, only DFT predicts mechanical response in close agreement with experimental data. In this regime, both the ramped and steady-state techniques discussed earlier show good agreement, while at lower pressures, the steady-state DFT method is in better agreement with experiment. As

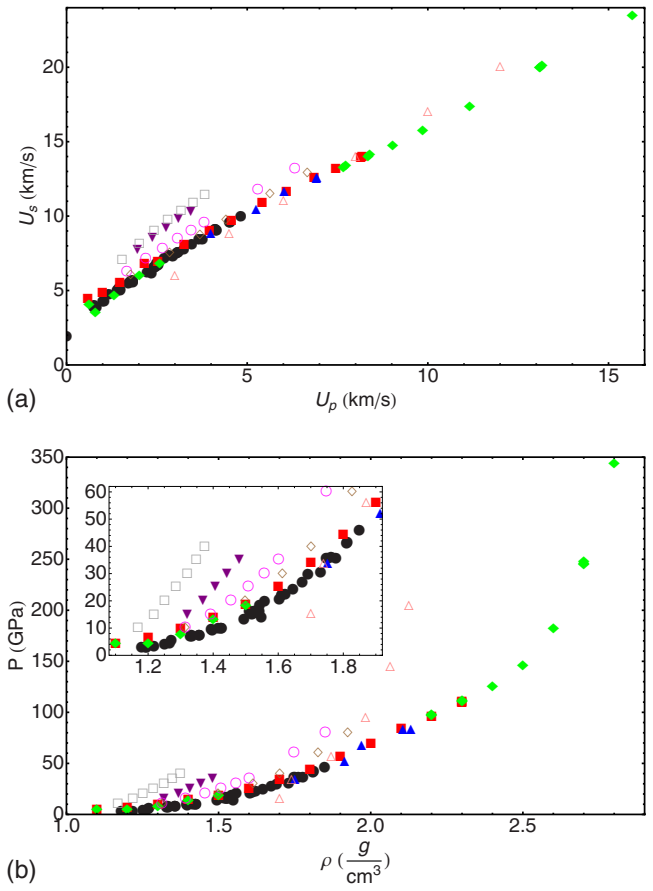


FIG. 3. (Color online) Hugoniot for polyethylene in $U_s$-$U_p$ (top) and P-$\rho$ (bottom). Experiments: shock handbook (Ref. 14) scaled to 0.955 g/cm$^3$ (black filled circles) and Nellis et al. (Ref. 10) (blue filled triangle up). Simulations: AIREBO (gray square), OPLS (purple filled triangle down), exp-6 (magenta circle), ReaxFF (brown diamond), tight-binding (Ref. 4) (pink triangles), DFT-AM05 temperature-ramp (red filled square), and DFT-AM05 steady-state (green filled diamond).

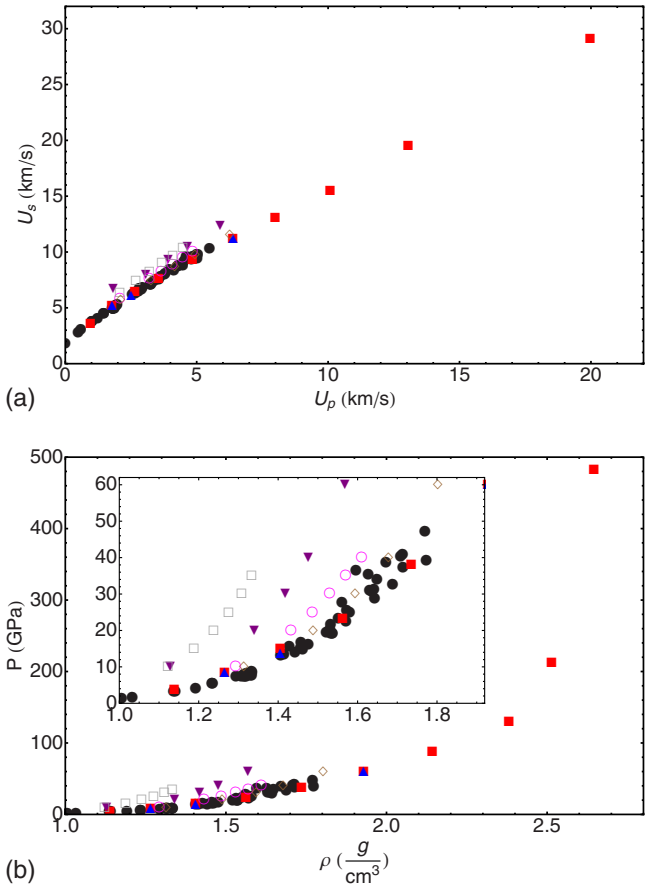


FIG. 4. (Color online) Hugoniot for poly(4-methyl-1-pentene) in $U_s$-$U_p$ (top) and P-$\rho$ (bottom). Experiment: shock handbook (Ref. 14) (black filled circle). Simulations: AIREBO (gray square), OPLS (purple filled triangle down), exp-6 (magenta circle), ReaxFF (brown diamond), DFT-AM05 geometry 1 (red filled square), and DFT-AM05 geometry 2 (blue filled triangle up).

a general rule, the classical potentials provide too stiff of a response at high pressures. At lower pressures, closer to ambient conditions where they are parametrized, the model potentials become more quantitatively accurate. Below 30 GPa, a density of 1.7 g/cm$^3$, ReaxFF deviates from DFT and experiment by less than 10%. Below 15 GPa, a density of 1.3 g/cm$^3$, the exp-6 potential gives reasonably good agreement. The OPLS and AIREBO potentials are decidedly too stiff; they do not offer accurate predictions for the mechanical loading at pressures significantly above a few GPa. Results from tight-binding calculations[4] are also shown in Fig. 3, demonstrating the long-standing challenge to predict properties for matter under shock compression.

#### *2. Poly(4-methyl-1-pentene)*

Our PMP Hugoniot results (see Fig. 4) demonstrate that the DFT simulations are in excellent agreement with experimental data, effectively capturing even the subtle curvature in $U_s$-$U_p$. As before, the ReaxFF potential is the most accurate classical potential, followed by the exp-6 potential. These are quantitatively accurate to within 10% at experimental pressures of 30 GPa and 15 GPa, respectively. The OPLS and AIREBO potentials have too stiff of a response in both hydrocarbon polymers even for very weak shocks. Since the OPLS potential does very well in describing normal and branched alkanes at ambient pressures,[49] this result suggest that the LJ 12–6 is in general too stiff[50] to model shocks; softer potentials such as the exp-6 appear to be more appropriate.

### B. Shock temperature

The temperature of the shocked state is important in determining the phase, rates of chemical reactions in the shock front, final equilibrium chemical composition, and transport properties such as thermal and electrical conductivity; it is, therefore, important to model and analyze also the shock temperature. The Hugoniot state can be viewed in the pressure-temperature plane, shown in Fig. 5. Although the stiffness of the Hugoniot in the pressure-density plane (Fig. 3) is also manifest in temperature density (Fig. 6), the P-T plot reveals that pressure and temperature, with minor exceptions, follow each other closely.

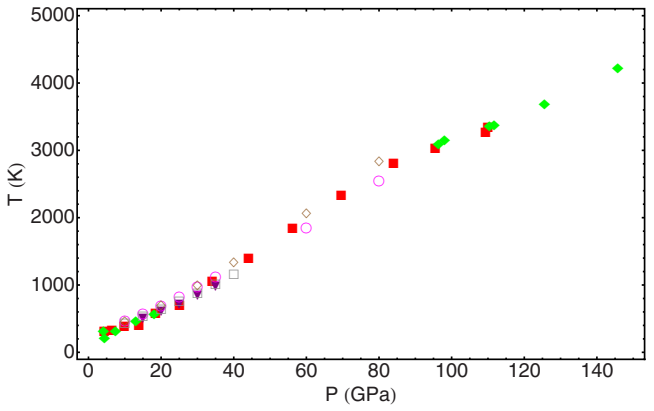


FIG. 5. (Color online) Calculated temperatures as a function of pressure along the polyethylene principal Hugoniot. AIREBO (gray square), OPLS (purple filled triangle down), exp-6 (magenta circle), ReaxFF (brown diamond), DFT-AM05 temperature-ramp (red filled square), and DFT-AM05 steady-state (green filled diamond).

A shock to a certain compression/density reaches a higher temperature and pressure when modeled in AIREBO or ReaxFF than it does in DFT. A shock to a certain pressure, on the other hand, will display similar temperature in DFT and the model potentials, but for strong shocks result in different compressions of the final state.

In Fig. 6, the calculated temperature along the Hugoniot is shown for polyethylene. The overall behavior of the shock temperature when comparing the different methods is analogous to that of the pressure. A particular shortcoming of classical potentials as well as ground-state/zero-Kelvin type DFT simulations is the lack of treatment of the effect of temperature on the electronic ground state, which results in a too stiff shock Hugoniot.[51] Since the DFT results for pressure are in agreement with experiments, we will in the following discussion compare the temperatures in the model potential simulations to those from DFT.

AIREBO yields too high temperature compared to the DFT results already for weak shocks, and the deviation grows rapidly with shock strength. The large discrepancy in temperature is particularly problematic for AIREBO since chemical reactivity depends sensitively on the temperature. If the DFT simulations of temperature are of high fidelity, it appears difficult to draw conclusions regarding chemical reactivity under shock conditions from simulations employing AIREBO.

ReaxFF, the second reactive potential investigated, instead shows behavior for compressions smaller than 50% (densities below 1.5 $g/cm^3$) that agree with DFT. For compressions beyond that, ReaxFF yields a higher shock temperature than DFT does. As discussed in the next section, these differences occur well below the threshold of dissociation, suggesting that ReaxFF could display significant uncertainties in predictions of chemical reactions resulting from stronger shocks.

Of the nonreactive potentials, exp-6 of Borodin *et al.* behaves well for shock compression below 1.5 $g/cm^3$ while the temperature rises rapidly compared to the DFT result for stronger shocks. The OPLS potential exhibits a rapid increase in shock temperature beginning already at 30% compression.

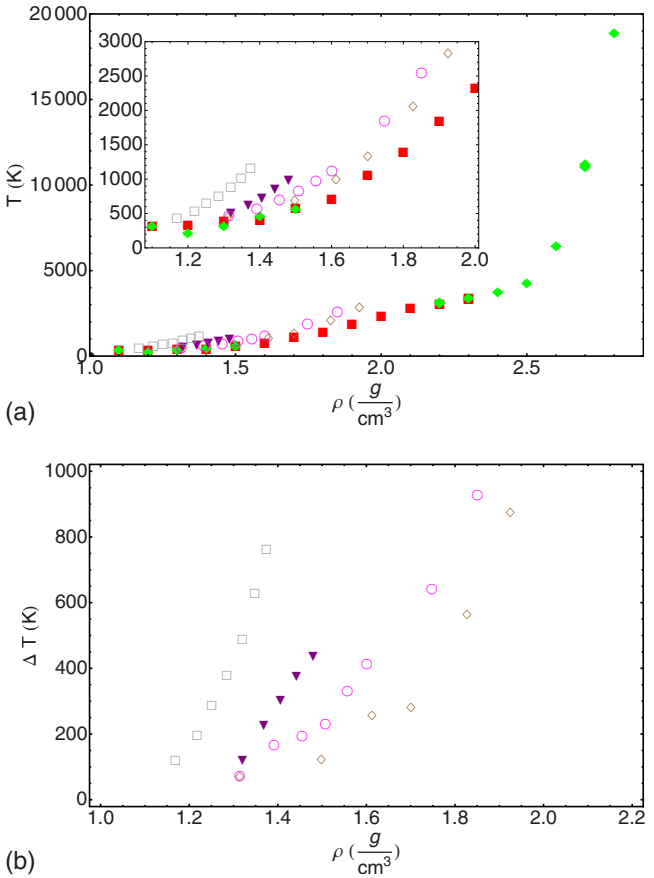


FIG. 6. (Color online) Calculated temperatures as a function of density along the polyethylene principal Hugoniot (top) and relative to the DFT-AM05 temperature (bottom). AIREBO (gray square), OPLS (purple filled triangle down), exp-6 (magenta circle), ReaxFF (brown diamond), DFT-AM05 temperature-ramp (red filled square), and DFT-AM05 steady-state (green filled diamond).

The DFT results show an interesting behavior at $2\frac{1}{2}$-fold compression (2.4 $g/cm^3$) where the temperature rise is suppressed. The feature is more pronounced in temperature than it is in pressure and $U_s$-$U_p$, although it is visible in the upper panel of Fig. 3 as a change in curvature at $U_p$=10 km/s. The reason is the gradual transition into the dissociated/atomic regime; the temperature increases rapidly again after dissociation is complete. The transition occurs at pressures greater than those of existing gas-gun experiments but is within the pressure range of laser or magnetically launched flyer plate driven experiments. We expect this range of shock compression to be investigated experimentally in the future.

### C. Chemical structure/dissociation

Shock induced dissociation is one of the aspects driving the transition into a dense plasma and is of particular interest due to the many changes associated with it. Although the ambient state of most polymers are electrical insulators, the dense dissociated state is conducting. This leads to substantial changes in thermophysical properties such as specific heat and thermal conductivity. From a computational perspective, the onset of dissociation determines the range of

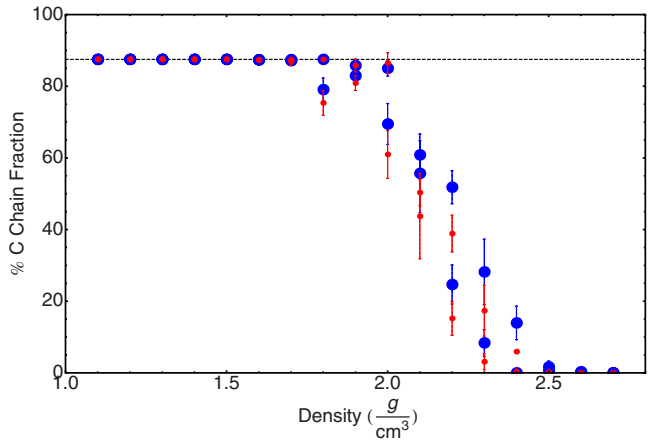


FIG. 7. (Color online) Average fraction of carbon atoms bound in the backbone in the DFT-AM05 simulations as a function of density along the Hugoniot. When there are two points at the same density, they are for two different temperatures bracketing the Hugoniot state. The error bars are one standard deviation. The cutoff distances used to define bonded atoms were 1.9 Å for C–C, 1.3 Å for C-H, and 0.8 Å for H-H. Results are shown for two cutoff times: 20 fs (large blue circle) and 50 fs (small red circle).

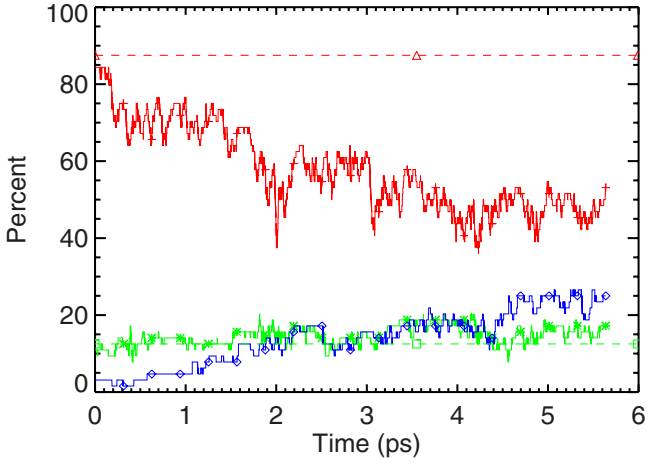


FIG. 8. (Color online) Distribution of carbon as a function of time in the DFT-AM05 simulation at 2.2 $g/cm^3$ along the Hugoniot at 3100 K presented as sliding averages over 10 fs intervals. Carbon in the backbone (red line +), carbon at the end of a strand (green line ∗), and carbon with three carbon neighbors (blue line ◇). The dashed lines show the fractions of perfect chains with 87.5% of carbon atoms in the backbone (red dashed triangle up) and 12.5% at the end of a strand (green dashed square). After 6 ps of equilibration, the backbone fraction has been reduced to 45% while 24% is bonded to three other carbons; the fraction of carbon atoms at the end of a strand fluctuates above the initial value. The composition changes over the first 3 ps as the system reaches equilibrium. During the last 3 ps, the count of backbone carbon atoms shows no trend, suggesting that the system can reach equilibrium over the time scale accessible in the first-principles simulations.

applicability for nonreactive potentials such as the Borodin exp-6 and OPLS.

We analyzed the DFT simulations for bond breaking by recording all neighbors within a cutoff distance of an atom and counting a bond as permanent/steady if it lasted longer than a cutoff time. Although the exact recorded chemical composition depends on the cutoff distances and time,[33] the estimation of the density where significant dissociation occurs is not sensitive to the choice of cutoff parameters.

Figure 7 shows the structural integrity of polyethylene along the Hugoniot as measured by the fraction of carbon atoms in a linear chain. Carbons in the chain will have two C and two H neighbors, except for the end atoms which will have one C and three H neighbors. The initial polyethylene strands are $C_{16}H_{34}$, hence the initial fraction of backbone carbon atoms is 14/16 or 87.5%. The polymer backbone is no longer intact when the ratio is reduced from that value, so by monitoring how the ratio changes, it is possible to follow the structural disintegration of the polymer.

In the time scale accessible to the DFT simulations, there is no appreciable dissociation below 1.8 $g/cm^3$ and no signature of a carbon back bone remaining above 2.5 $g/cm^3$. The region of partial dissociation (2.2–2.4 $g/cm^3$) corresponds directly to the plateau in temperature along the pressure Hugoniot shown in Fig. 6 and the inflection in the $U_s$-$U_p$ relation of Fig. 3.

Under compression, the linear chains break up and structures of carbon atoms with three or more carbon neighbors begin to emerge. An example of that is shown in Fig. 8, where the character of carbon atoms at 2.2 $g/cm^3$ and 3100 K is plotted as a function of time. At even higher compression, $H_2$ molecules begin to form and carbon-carbon coordination becomes more pronounced.

## V. CONCLUSIONS

We have simulated the behavior under shock compression for two polymers using DFT based molecular dynamics with the AM05 density functional and four different classical force-fields. We conclude that the response to weak shocks in both PE and PMP are well described by the exp-6 of Borodin *et al.* and ReaxFF force-fields, with the latter being valid over a larger range in density and pressure. OPLS and AIREBO both yield significantly too high pressure along the Hugoniot already for weak shocks. For strong shocks, only the DFT based simulations are of high fidelity when compared to existing experimental data up to 80 GPa. Based on the first-principles simulations, we predict a feature in the polyethylene Hugoniot at $U_p$=10 km/s due to gradual dissociation between 2.2 and 2.5 $g/cm^3$.

It is notable that all of the classical model potentials tested begin deviating from the DFT simulations at significantly lower densities, pressures, and temperatures than those required for bonds to break. This finding carries implications for future development of force-fields, both reactive and nonreactive. Nonreactive force fields for hydrocarbons have a potential maximum range of validity in shock applications of 1.8 $g/cm^3$, but an improved fidelity for high density will require changes in the nonbonded interaction parameterization. The behavior of AIREBO is incorrect when compared to experimental data for pressure at 20% compression, 1.2 $g/cm^3$, a region where no dissociation occurs in the DFT

simulations, implying that significant revisions are necessary for the potential to be useful for shock problems. ReaxFF has a longer range of validity when compared to experimental pressure data for both PE and PMP, but the temperature difference to DFT above 1.9 $g/cm^3$ is a point of concern for shock applications.

We expect that the results outlined throughout this paper will encourage large-scale DFT simulations of macromolecular systems for shock applications. The findings can also provide guidance when it comes to selecting interaction potentials for work employing classical molecular dynamics simulations to study shocks in organic materials in general and hydrocarbon polymers in particular.

## ACKNOWLEDGMENTS

We thank P. in't Veld for generating the large PE sample, G. Kresse for the early opportunity to employ VASP 5.1, P. Kent for sharing Cray XT4 code modifications,[52] and S. Stuart and S. Zybin for discussions on AIREBO. The work was supported by the NNSA Science Campaigns. This work was supported by the Laboratory Directed Research and Development program at Sandia National Laboratories. Sandia is a multiprogram laboratory operated by Sandia Corporation, a Lockheed Martin Company, for the United States Department of Energy's National Nuclear Security Administration under Contract No. DE-AC04-94AL85000.

[1] M. D. Knudson, D. L. Hanson, J. E. Bailey, C. A. Hall, J. R. Asay, and W. W. Anderson, Phys. Rev. Lett. **87**, 225501 (2001).
[2] M. P. Desjarlais, Phys. Rev. B **68**, 064204 (2003).
[3] M. D. Knudson, M. P. Desjarlais, and D. H. Dolan, Science **322**, 1822 (2008).
[4] J. D. Kress, S. R. Bickham, L. A. Collins, B. L. Holian, and S. Goedecker in *Shock Compression of Condensed Matter-1999*, edited by M. D. Furnish, L. C. Chhabildas, and R. S. Hixson, AIP Conference Proceedings Vol. 505 (AIP, New York, 2000), p. 381.
[5] P. Hohenberg and W. Kohn, Phys. Rev. **136**, B864 (1964); W. Kohn and L. J. Sham, *ibid.* **140**, A1133 (1965).
[6] K. Chenoweth, A. C. T. van Duin, and W. A. Goddard III, J. Phys. Chem. A **112**, 1040 (2008).
[7] S. J. Stuart, A. B. Tutein, and J. A. Harrison, J. Chem. Phys. **112**, 6472 (2000).
[8] W. L. Jorgensen, D. S. Maxwell, and J. Tirado-Rives, J. Am. Chem. Soc. **118**, 11225 (1996).
[9] O. Borodin and G. D. Smith, J. Phys. Chem. B **110**, 6279 (2006); O. Borodin, G. D. Smith, and D. Bedrov, *ibid.* **106**, 9912 (2002).
[10] W. J. Nellis, F. H. Ree, R. J. Trainor, A. C. Mitchell, and M. B. Boslough, J. Chem. Phys. **80**, 2789 (1984).
[11] J. C. F. Millett and N. K. Bourne, J. Phys. D **37**, 2901 (2004).
[12] N. K. Bourne, J. C. F. Millett, and S. G. Goveas, J. Phys. D **40**, 5714 (2007).
[13] N. K. Bourne and J. C. F. Millett, J. Mater. Sci. **43**, 185 (2008).
[14] *LASL Shock Hugoniot Handbook*, edited by S. P. March (University of California Press, Berkeley, CA, 1980).
[15] M. L. Elert, S. V. Zybin, and C. T. White, J. Chem. Phys. **118**, 9795 (2003).
[16] S. Zybin, M. Elert, and C. White, in *Shock Compression of Condensed Matter-2003*, edited by M. D. Furnish, Y. M. Gupta, and J. W. Forbes, AIP Conference Proceedings Vol. 706 (AIP, New York, 2004), pp. 306–309.
[17] L. Zhang, S. V. Zybin, A. C. T. van Duin, S. Dasgupta, and W. A. Goddard III, in *Shock Compression of Condensed Matter-2005*, edited by M. D. Furnish, M. Elert, T. Russell, and C. White, AIP Conference Proceedings Vol. 845 (AIP, New York, 2006), p. 589.
[18] S. J. Plimpton, J. Comput. Phys. **117**, 1 (1995).
[19] LAMMPS MD code http://lammps.sandia.gov.
[20] P. E. Blöchl, Phys. Rev. B **50**, 17953 (1994); G. Kresse and D. Joubert, *ibid.* **59**, 1758 (1999).
[21] G. Kresse and J. Hafner, Phys. Rev. B **47**, 558 (1993); **49**, 14251 (1994); G. Kresse and J. Furthmüller, *ibid.* **54**, 11169 (1996).
[22] R. Armiento and A. E. Mattsson, Phys. Rev. B **72**, 085108 (2005).
[23] A. E. Mattsson, R. Armiento, J. Paier, G. Kresse, J. M. Willis, and T. R. Mattsson, J. Chem. Phys. **128**, 084714 (2008).
[24] P. Haas, F. Tran, and P. Blaha, Phys. Rev. B **79**, 085104 (2009).
[25] J. Paier, M. Marsman, K. Hummer, G. Kresse, I. C. Gerber, and J. G. Angyan, J. Chem. Phys. **124**, 154709 (2006).
[26] J. Paier, M. Marsman, K. Hummer, G. Kresse, I. C. Gerber, and J. G. Angyan, J. Chem. Phys. **125**, 249901 (2006).
[27] A. E. Mattsson and T. R. Mattsson, J. Chem. Theory Comput. **5**, 887 (2009).
[28] R. P. Muller, A. E. Mattsson, and C. L. Janssen, J. Comput. Chem. e-print arXiv:0908.1744v3.
[29] E. F. C. Byrd and B. Rice, J. Phys. Chem. C **111**, 2787 (2007).
[30] A. E. Mattsson, R. R. Wixom, and T. R. Mattsson (unpublished).
[31] M. D. Knudson and M. P. Desjarlais, Phys. Rev. Lett. **103**, 225501 (2009).
[32] A. E. Mattsson, P. A. Schultz, M. P. Desjarlais, T. R. Mattsson, and K. Leung, Modell. Simul. Mater. Sci. Eng. **13**, R1 (2005).
[33] T. R. Mattsson and M. P. Desjarlais, Phys. Rev. Lett. **97**, 017801 (2006).
[34] See supplementary material at http://link.aps.org/supplemental/10.1103/PhysRevLett.97.017801.
[35] The use of a high-cutoff energy (ENMAX*2.0) and volume changes of the order 10% minimize Pulay errors: http://cms.mpi.univie.ac.at/vasp/vasp/node214.html.
[36] S. Rempe, T. R. Mattsson, and K. Leung, Phys. Chem. Chem. Phys. **10**, 4685 (2008).
[37] N. Mermin, Phys. Rev. **137**, A1441 (1965).
[38] A. Strachan, A. van Duin, D. Chakraborty, S. Dasgupta, and W. A. Goddard III, Phys. Rev. Lett. **91**, 098301 (2003).
[39] J. Budzien, A. P. Thompson, and S. V. Zybin, J. Phys. Chem. B **113**, 13142 (2009).
[40] W. L. Jorgensen, J. D. Madura, and C. J. Swenson, J. Am. Chem. Soc. **106**, 6638 (1984).

[41] R. W. Hockney and J. W. Eastwood, *Computer Simulation Using Particles* (Adam Hilger-IOP, Bristol, 1988).
[42] F. Pierce, M. Tsige, O. Borodin, D. Perahia, and G. S. Grest, J. Chem. Phys. **128**, 214903 (2008).
[43] Accelrys Materials Studio, http://accelrys.com/.
[44] A. Liu and S. J. Stuart, J. Comput. Chem. **29**, 601 (2008).
[45] M. B. Boslough and J. R. Asay, in *High-Pressure Phock Compression of Solids*, edited by J. R. Asay and M. Shahinpoor (Springer-Verlag, New York, 1993), p. 7.
[46] R. Ravelo, B. L. Holian, T. C. Germann, and P. S. Lomdahl, Phys. Rev. B **70**, 014103 (2004).
[47] M. French, T. R. Mattsson, N. Nettelmann, and R. Redmer, Phys. Rev. B **79**, 054107 (2009).
[48] T. R. Mattsson and R. J. Magyar, in *Shock Compression of Condensed Matter-2009*, edited by M. L. Elert W. T. Buttler, M. D. Furnish, W. W. Anderson, and W. G. Proud, AIP Conference Proceedings, Vol. 1195 (AIP, New York, 2009), pp. 797–800.
[49] A. E. Ismail and M. Tsige, P. J. in't Veld, and G. S. Grest, Mol. Phys. **105**, 3155 (2007).
[50] A. Warshel and S. Lifson, J. Chem. Phys. **53**, 582 (1970).
[51] W. J. Nellis, M. vanThiel, and A. C. Mitchell, Phys. Rev. Lett. **48**, 816 (1982).
[52] P. R. C. Kent, J. Phys.: Conf. Ser. **125**, 012058 (2008).